Impedance Characterization of a Two-Post Mounting Structure for Varactor-Tuned Gunn Oscillators

OSMAN L. EL-SAYED

Abstract—**A lumped equivalent circuit is used to characterize a two-post waveguide mounting structure frequently utilized in varactor-tuned Gunn oscillators. Analytical expressions for the different elements are derived. Comparison with experimental results enabled us to refine the model by the introduction of correction factors which compensate for the simplifying assumptions of the theoretical model. This equivalent circuit would facilitate the optimization of the performance of this type of oscillator.**

I. INTRODUCTION

IT IS common knowledge that the mode of operation of active microwave semiconductor diodes (Gunn, IMPATT, varactor) is strongly dependent on the impedance presented at their terminals, not only at the fundamental frequency, but also at its harmonics. Thus accurate impedance characterization of their mounting structure is necessary to achieve performance optimization.

In typical mounting structures for full-height varactor-tuned Gunn oscillators, the tuning is achieved either in a series or parallel fashion [1]–[3]. In the first type, both the Gunn and varactor diodes are post-mounted in line within the guide. Tight coupling of both devices is only achieved in a limited range of frequencies and hence a rather limited tuning range is possible.

In the second type both devices are mounted under separate posts positioned across the cross section of the guide [Fig. 1(a)]. Up until now no circuit model was devised for this structure and oscillator design remained empirical. The achievement of such a circuit model is our main concern in this paper. A symmetrical configuration is chosen in order to put the problem in a manageable form [Fig. 1(b)].

II. MOUNTING STRUCTURE ANALYSIS

This analysis follows the general procedure adopted by Eisenhart and Khan [4] for single post mounts and extends it to the two-post mounting structure. In general, the gaps are driven by voltages different in modulus and phase (V^{I},V^{II}) resulting in different gap fields and post currents. This general case is reduced to a linear combination of the cases of symmetric and antisymmetric gap drives which will be simultaneously analyzed. Superscripts s and a will distinguish the quantities relevant to each case. Quantities relevant to the general case will have no superscript. It should be noted that the analysis deals (as in [4]) with thin flat posts.

Manuscript received July 18, 1973; revised March 27, 1974.
The author is with the Department of Electronics, University of Provence, Center of Saint-Jerome, Marseille, France.

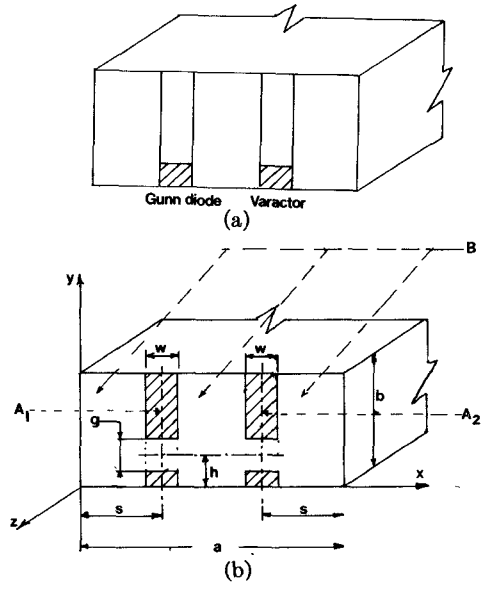

Fig. 1. (a) General structure under analysis. (b) Typical parallel-type varactor-tuned Gunn oscillator.

A. Dyadic Green's Function $G(r \mid r')$

It is given by [4]

$$G(r \mid r') = \sum_{n=0}^{\infty} \sum_{m=1}^{\infty} \frac{(2-\delta_n)(k^2-k_y^2)\exp(-\Gamma_{mn} \mid z-z' \mid)}{abk^2\Gamma_{mn}} \cdot \sin k_x x \sin k_x x' \cos k_y y \cos k_y y' \quad (1)$$

where

$$k_x = \frac{m\Pi}{a} \quad k_y = \frac{n\Pi}{b} \quad k = \frac{2\Pi}{\lambda}$$

$$\Gamma_{mn} = (k_x^2 + k_y^2 - k^2)^{1/2}$$

$$\delta_n = \begin{cases} 1, & \text{for } n = 0 \\ 0, & \text{for } n \neq 0. \end{cases}$$

B. Current Density $J(r)$

In the general case, the current densities in the two posts ($J^{I}(y)$,$J^{II}(y)$) differ, in general, in modulus and

phase. They will be assumed uniformly distributed across the posts but will have different spatial distributions along them. It can be easily shown that the general case can be expressed in terms of symmetric and antisymmetric components.

$$J^s(r) = \hat{y}\, 2J_0{}^s u^s(y) u^s(x) \delta(z-0) \tag{2a}$$

$$J^a(r) = \hat{y}\, 2J_0{}^a u^a(y) u^a(x) \delta(z-0) \tag{2b}$$

$$J(r) = J^s(r) + J^a(r) \tag{2c}$$

where

$$u^s(y) = \sum_{l=0}^{\infty} \frac{(2-\delta_l)}{b}\left(A_l{}^{y,s}\cos\frac{l\Pi y}{b} + B_l{}^{y,s}\sin\frac{l\Pi y}{b}\right) \tag{2d}$$

$$u^a(y) = \sum_{l=0}^{\infty} \frac{(2-\delta_l)}{b}\left(A_l{}^{y,a}\cos\frac{l\Pi y}{b} + B_l{}^{y,a}\sin\frac{l\Pi y}{b}\right) \tag{2e}$$

$$u^s(x) = \sum_{f=0}^{\infty} \frac{(2-\delta_f)}{a}\left(A_f{}^{x,s}\cos\frac{f\Pi x}{a} + B_f{}^{x,s}\sin\frac{f\Pi x}{a}\right) \tag{2f}$$

$$u^a(x) = \sum_{f=0}^{\infty} \frac{(2-\delta_f)}{a}\left(A_f{}^{x,a}\cos\frac{f\Pi x}{a} + B_f{}^{x,a}\sin\frac{f\Pi x}{a}\right) \tag{2g}$$

where the normalized expansion coefficients are given by:

$$A_f{}^{x,s} = \begin{cases} w\cos\left(\dfrac{f\Pi s}{a}\right)\dfrac{\sin\theta_f}{\theta_f}, & \text{for } f \text{ even, zero included} \\ 0, & \text{for } f \text{ odd} \end{cases}$$

$$A_f{}^{x,a} = \begin{cases} w\cos\left(\dfrac{f\Pi s}{a}\right)\dfrac{\sin\theta_f}{\theta_f}, & \text{for } f \text{ odd} \\ 0, & \text{for } f \text{ even, zero included} \end{cases}$$

$$B_f{}^{x,s} = \begin{cases} w\sin\left(\dfrac{f\Pi s}{a}\right)\dfrac{\sin\theta_f}{\theta_f}, & \text{for } f \text{ odd} \\ 0, & \text{for } f \text{ even} \end{cases}$$

$$B_f{}^{x,a} = \begin{cases} w\sin\left(\dfrac{f\Pi s}{a}\right)\dfrac{\sin\theta_f}{\theta_f}, & \text{for } f \text{ even} \\ 0, & \text{for } f \text{ odd} \end{cases}$$

$$\theta_f = \frac{f\Pi w}{2a}$$

$$A_l{}^{y,s}J_0{}^s = \tfrac{1}{2}(A_l{}^{y,\mathrm{I}}J_0{}^{\mathrm{I}} + A_l{}^{y,\mathrm{II}}J_0{}^{\mathrm{II}})$$

$$B_l{}^{y,s}J_0{}^s = \tfrac{1}{2}(B_l{}^{y,\mathrm{I}}J_0{}^{\mathrm{I}} + B_l{}^{y,\mathrm{II}}J_0{}^{\mathrm{II}})$$

$$A_l{}^{y,a}J_0{}^a = \tfrac{1}{2}(A_l{}^{y,\mathrm{I}}J_0{}^{\mathrm{I}} - A_l{}^{y,\mathrm{II}}J_0{}^{\mathrm{II}})$$

$$B_l{}^{y,a}J_0{}^a = \tfrac{1}{2}(B_l{}^{y,\mathrm{I}}J_0{}^{\mathrm{I}} - B_l{}^{y,\mathrm{II}}J_0{}^{\mathrm{II}}) \tag{3}$$

for all l from 0 to ∞.

$A_l{}^{y,\mathrm{I}}, B_l{}^{y,\mathrm{I}}, A_l{}^{y,\mathrm{II}}, B_l{}^{y,\mathrm{II}}$ are normalized expansion coefficients of the current density distributions along the posts (I) and II in the general case.

C. Electric Field $E(r)$ in the Whole Region Defined by the Guide

$$E(r) = -j\omega\mu_0 \int G(r \mid r')J(r')\, dV'$$

$$E^s(r) = -\frac{\hat{y}2j\eta J_0{}^s}{abk}\sum_{n=0}^{\infty}\sum_{m=1,3,\mathrm{odd}}^{\infty}\frac{(2-\delta_n)(k^2-k_y{}^2)}{\Gamma_{mn}} \cdot A_n{}^{y,s}B_m{}^{x,s}\sin k_x x\cos k_y y\exp(-\Gamma_{mn}\mid z\mid) \tag{4a}$$

$$E^a(r) = \frac{-\hat{y}2j\eta J_0{}^a}{abk}\sum_{n=0}^{\infty}\sum_{m=2,4;\mathrm{even}}^{\infty}\frac{(2-\delta_n)(k^2-k_y{}^2)}{\Gamma_{mn}} \cdot A_n{}^{y,a}B_m{}^{x,a}\sin k_x x\cos k_y y\exp(-\Gamma_{mn}\mid z\mid) \tag{4b}$$

$$E(r) = E^s(r) + E^a(r). \tag{4c}$$

D. Gap Field E_a

The gap fields are assumed uniform in both x and y directions. Expanding them in terms of spatial harmonic functions we get:

$$E_a{}^s = -\hat{y}\frac{V^s}{g}v(y)v^s(x)\delta(z-0) \tag{5a}$$

$$E_a{}^a = -\hat{y}\frac{V^a}{g}v(y)v^a(x)\delta(z-0) \tag{5b}$$

$$E_a = E_a{}^s + E_a{}^a \tag{5c}$$

where

$$v(y) = \sum_{p=0}^{\infty}\left(\frac{2-\delta_p}{b}\right)S_p\cos\frac{p\Pi y}{b} \tag{5d}$$

$$S_p = g\cos\frac{p\Pi h}{b}\frac{\sin\Phi_p}{\Phi_p} \tag{5e}$$

$$\Phi_p = \frac{p\Pi g}{2b} \tag{5f}$$

$$V^s = \tfrac{1}{2}(V^{\mathrm{I}} + V^{\mathrm{II}}) \quad V^a = \tfrac{1}{2}(V^{\mathrm{I}} - V^{\mathrm{II}}) \tag{5g}$$

$$v^s(x) = \begin{cases} 1, & \text{for } (s-w/2) < x < (s+w/2) \text{ and } (a-s-w/2) < x < (a-s+w/2) \\ 0, & \text{elsewhere} \end{cases} \tag{5h}$$

$$v^a(x) = \begin{cases} 1, & \text{for } (s-w/2) < x < (s+w/2) \\ -1, & \text{for } (a-s-w/2) < x < (a-s+w/2) \\ 0, & \text{elsewhere.} \end{cases} \tag{5i}$$

E. Spatial Harmonic Functions

Since the tangential electric field at the surface of a perfectly conducting antenna is equal to zero, an integration of the product $E_r \cdot J_r$ over the surface of the antenna will clearly give a null. Thus the power is actually radiated

from the antenna feed and is merely "guided" by the antenna structure [6]. Therefore, the power radiated as calculated using Carters induced EMF method (subject to all its limitations) is equal to the power incident on the gaps.

$$\int E_a J(r)\,dxdydz = \int E(r)J(r)\,dxdydz \tag{5j}$$

over A_1, A_2 over the volume enclosed by guide

$$(\text{LHS})^s = -2\sum_{n=0}^{\infty} V^s\left(\frac{2-\delta_n}{b}\right)J_0{}^s w A_n{}^{y,s}\cos k_y h\,\frac{\sin\Phi_n}{\Phi_n}$$

$$= -2\sum_{n=0}^{\infty} V^s I_n{}^s$$

$$= -2\sum_{n=0}^{\infty} P_n{}^s \tag{6a}$$

$$(\text{LHS})^a = -2\sum_{n=0}^{\infty} V^a\left(\frac{2-\delta_n}{b}\right)J_0{}^a w A_n{}^{y,a}\cos k_y h\,\frac{\sin\Phi_n}{\Phi_n}$$

$$= -2\sum_{n=0}^{\infty} V^a I_n{}^a$$

$$= -2\sum_{n=0}^{\infty} P_n{}^a \tag{6b}$$

where

$$I_n{}^s = \left(\frac{2-\delta_n}{b}\right)J_0{}^s w A_n{}^{y,s}\cos k_y h\,\frac{\sin\Phi_n}{\Phi_n}$$

$$= \tfrac{1}{2}(I_n{}^{\mathrm{I}} + I_n{}^{\mathrm{II}}) \tag{6c}$$

$$I_n{}^a = \left(\frac{2-\delta_n}{b}\right)J_0{}^a w A_n{}^{y,a}\cos k_y h\,\frac{\sin\Phi_n}{\Phi_n}$$

$$= \tfrac{1}{2}(I_n{}^{\mathrm{I}} - I_n{}^{\mathrm{II}}) \tag{6d}$$

$$(\text{RHS})^s = -2\sum_{n=0}^{\infty}\sum_{m=1,3;\,\text{odd}}^{\infty} j \cdot \frac{2(2-\delta_n)\eta(A_n{}^{y,s}J_0{}^s)^2 w^2(k^2-k_y{}^2)}{abk\Gamma_{mn}} \cdot \sin^2 k_x s\left(\frac{\sin\theta_m}{\theta_m}\right)^2 \tag{7a}$$

$$(\text{RHS})^a = -2\sum_{n=0}^{\infty}\sum_{m=2,4;\,\text{even}}^{\infty} j \cdot \frac{2(2-\delta_n)\eta(A_n{}^{y,a}J_0{}^a)^2 w^2(k^2-k_y{}^2)}{abk\Gamma_{mn}} \cdot \sin^2 k_x s\left(\frac{\sin\theta_m}{\theta_m}\right)^2. \tag{7b}$$

From equations (6a), (6b), (7a), and (7b):

$$P_n{}^s = j\frac{2(2-\delta_n)\eta(A_n{}^{y,s}J_0{}^s)^2 w^2(k^2-k_y{}^2)}{abk} \cdot \sum_{m=1,3;\,\text{odd}}^{\infty}\frac{\sin^2 k_x s(\sin\theta_m/\theta_m)^2}{\Gamma_{mn}} \tag{8a}$$

$$P_n{}^a = j\frac{2(2-\delta_n)\eta(A_n{}^{y,a}J_0{}^a)^2 w^2(k^2-k_y{}^2)}{abk} \cdot \sum_{m=2,4;\,\text{even}}^{\infty}\frac{\sin^2 k_x s(\sin\theta_m/\theta_m)^2}{\Gamma_{mn}}. \tag{8b}$$

Defining

$Z_r \equiv$ gap driving point impedance;

$Z_n \equiv$ gap driving point impedance related to the nth spatial harmonic.

$$\sum_{n=0}^{\infty} P_n = \frac{V^2}{Z_r} = \sum_{n=0}^{\infty}\frac{V^2}{Z_n}$$

$$\frac{1}{Z_r} = \sum_{n=0}^{\infty}\frac{1}{Z_n}.$$

Since $Z_n = P_n/I_n{}^2$ we have from (6c), (6d), (8a), and (8b):

$$Z_n{}^s = \frac{1}{Y_n{}^s} = j\eta\frac{2b}{a}\frac{k^2-k_y{}^2}{(2-\delta_n)k}\sum_{m=1,3;\,\text{odd}}^{\infty}\frac{k_{pm}{}^2/k_{gn}{}^2}{\Gamma_{mn}} \tag{9a}$$

$$Z_n{}^a = \frac{1}{Y_n{}^a} = j\eta\frac{2b}{a}\frac{k^2-k_y{}^2}{(2-\delta_n)k}\sum_{m=2,4;\,\text{even}}^{\infty}\frac{k_{pm}{}^2/k_{gn}{}^2}{\Gamma_{mn}} \tag{9b}$$

where

$$k_{pm} = \sin k_x s\,\frac{\sin\theta_m}{\theta_m} \tag{9c}$$

$$k_{gn} = \cos k_y h\,\frac{\sin\Phi_n}{\Phi_n}. \tag{9d}$$

F. Determination of Equivalent Circuit Components

If we consider the mounting structure as two coupled antennas, a coupling network for each n spatial harmonic may be postulated. The complete equivalent circuit will consist of an infinite number of such coupling circuits corresponding to all values of n from 0 to ∞, connected in parallel between the two gaps. Π coupling networks might seem more appropriate than T's. We shall see however that the use of T coupling networks, at least for $n = 0$, gives a better physical insight of the problem. We define the following.

$Z_{1(n)} \equiv$ The series impedance of the T coupling network related to the nth spatial mode.

$Z_{2(n)} \equiv$ The shunt arm impedance of the T coupling network related to the nth spatial mode.

It may be easily shown that $Z_{1(n)}$ and $Z_{2(n)}$ are given by:

$$Z_{1(n)} = Z_n{}^a \tag{10a}$$

$$Z_{2(n)} = \tfrac{1}{2}(Z_n{}^s - Z_n{}^a). \tag{10b}$$

From (9a) and (9b) we get:

$$Z_{1(n)} = j\eta \frac{2b}{a} \frac{k^2 - k_y{}^2}{(2 - \delta_n)k} \sum_{m=2,4;\text{even}}^{\infty} \frac{k_{pm}{}^2/k_{gn}{}^2}{\Gamma_{mn}} \tag{11a}$$

$$Z_{2(n)} = j\eta \frac{b}{a} \frac{k^2 - k_y{}^2}{(2 - \delta_n)k} \sum_{m=1}^{\infty} (-)^{m+1} \frac{k_{pm}{}^2/k_{gn}{}^2}{\Gamma_{mn}}. \tag{11b}$$

For $n = 0$ [Fig. 2(a)]:

$$Z_{1(0)} = j\eta \frac{2b}{a} k \sum_{m=2,4;\text{even}}^{\infty} \frac{k_{pm}{}^2}{\Gamma_{m0}} \tag{12a}$$

$$Z_{2(0)} = \frac{1}{2}\left[\frac{2b}{a}\eta \frac{k}{k'}\right] k_{p1}{}^2 + j\eta \frac{b}{a} \sum_{m=2}^{\infty} (-)^{m+1} \frac{k_{pm}{}^2}{\Gamma_{m0}} \tag{12b}$$

where $jk' = \Gamma_{10}$.

For the dominant mode (TE_{10}) it is evident that the first term in the expression of $Z_{2(0)}$ above is real and corresponds to half the characteristic impedance of the guide referred to the post position. It is convenient to interpret it as being the parallel combination of the impedances presented by the guide at the plane $z = 0$ for both directions of propagation. The T network may thus be redrawn as in Fig. 2(b), where this impedance term is represented as a termination on the mount, thus permitting the handling of the mount as an obstacle in the guide. This representation is very convenient since all our experimental work is based on the measurement of the mount impedance considered as an obstacle in the guide. Such a representation is not possible if a Π coupling network is used.

Π coupling networks may be used for $n > 0$ and combined in parallel [Fig. 3(a)] yielding a single network whose shunt and series admittances are given, respectively, by:

$$Y_c = \frac{1}{Z_c} = \sum_{n=1}^{\infty} Y_n{}^s = \sum_{n=1}^{\infty} \left(j\eta \frac{b}{a} \frac{k^2 - k_y{}^2}{k} \cdot \sum_{m=1,3;\text{odd}}^{\infty} \frac{k_{pm}{}^2/k_{gn}{}^2}{\Gamma_{mn}} \right)^{-1} \tag{13a}$$

$$Y_s = \frac{1}{Z_s} = \sum_{n=1}^{\infty} \tfrac{1}{2}(Y_n{}^a - Y_n{}^s) = \sum_{n=1}^{\infty} \left\{ \left(j2\eta \frac{b}{a} \frac{k^2 - k_y{}^2}{k} \cdot \sum_{m=2,4;\text{even}}^{\infty} \frac{k_{pm}{}^2/k_{gn}{}^2}{\Gamma_{mn}} \right)^{-1} - \left(j2\eta \frac{b}{a} \frac{k^2 - k_y{}^2}{k} \sum_{m=1,3}^{\infty} \frac{k_{pm}{}^2/k_{gn}{}^2}{\Gamma_{mn}} \right)^{-1} \right\}. \tag{13b}$$

The Π coupling network thus obtained is combined with the "rearranged" T coupling network (corresponding to $n = 0$) as shown in Fig. 3(b) to give the complete equivalent circuit. In order to put it in manageable form the △ network formed by $Z_{1(0)}$, $Z_{1(0)}$, and Z_s is transformed to a Y network giving the final equivalent circuit Fig. 4 where

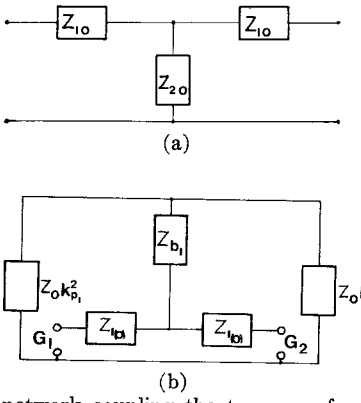

Fig. 2. (a) T network coupling the two gaps for $n = 0$. (b) Rearranged T coupling network for $n = 0$.

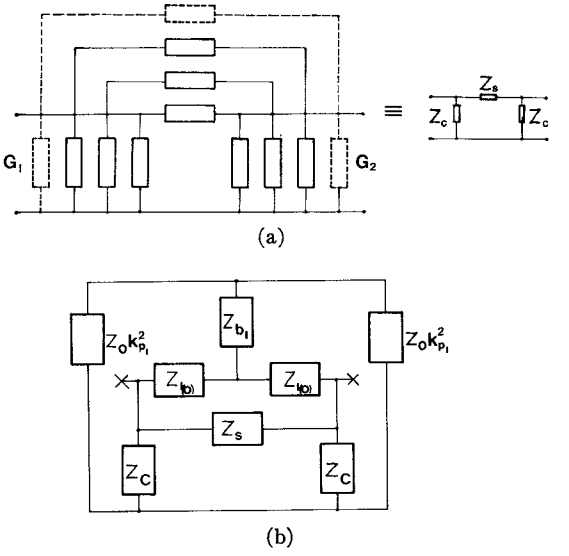

Fig. 3. (a) Π coupling networks for all $n > 0$. (b) Complete equivalent circuit combining the coupling network for $n = 0$ [Fig. 2(b)] and the coupling networks for all n from 1 to ∞ [Fig. 3(a)].

$$Z_a = \frac{Z_{1(0)}Z_s}{2Z_{1(0)} + Z_s} \tag{14a}$$

$$Z_{b2} = \frac{Z_{1(0)}{}^2}{2Z_{1(0)} + Z_s} \tag{14b}$$

$$Z_b = Z_{b1} + Z_{b2} \tag{14c}$$

where Z_{b1} is the second term in the expression of $Z_{2(0)}$ [see 12(b)].

If this circuit is to be referred to the center of the guide the impedances of all the components should be divided by $k_{p1}{}^2$.

Considered as an obstacle the mount should therefore present an impedance Z_{obs} given by:

$$Z_{\text{obs}} = \frac{1}{k_{p1}{}^2}\left[Z_b + \frac{1}{2}\left(Z_a + \frac{Z_cZ_g}{Z_c + Z_g}\right)\right] \tag{15}$$

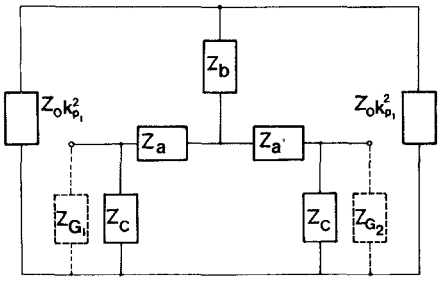

Fig. 4. Final theoretical equivalent circuit after Δ/Y transformation.

where Z_g is the impedance of the devices (assumed identical) present between the gap terminals. In the case where the gaps are left open, Z_g will represent the gaps static capacitances. They will be considered equivalent to a parallel plate capacitance whose area is the post X-sectional area and separation is the gap separation g.

III. THEORETICAL DISCUSSION

Many simplifying assumptions have been made all through the above analysis.

Assumptions of uniform current density across the posts and uniform spatial distribution of gap fields were made in [4]. However, they might not remain valid in the same ranges since in our case two posts are present in the same cross section. It is to be expected that the range of post widths within which the assumption of uniform current density remains valid will depend mainly on post position(s), operating frequency, and field distribution in the vicinity of the posts and will only be practically accessible through experimental measurements. As for the assumption of uniform spatial distribution of the gap fields in the y direction, it is expected that it will remain valid within the same range found in [4], i.e., in the range $g < b/4$. This, however, has to be checked by experimental measurements.

In the case of unequal gap loads, the analysis still holds since the post currents and the gap fields (or voltages) could be expressed in terms of symmetric and antisymmetric components as long as the above assumptions are valid. Furthermore, the variational form in which the impedances are expressed will tend to reduce the effects of deviations of current density distribution along the posts from the assumed ones.

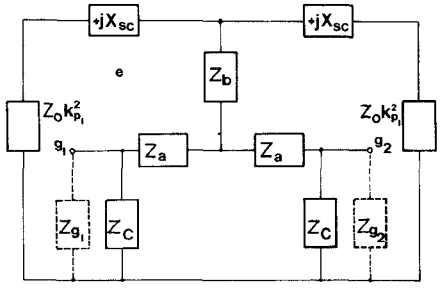

Fig. 5. Final equivalent circuit (including the series capacitive reactances X_{sc} which correct the effect of phase variation of incident wave across the posts).

As for convergence properties of the impedance functions they were fully discussed in [4]. However, in our case, we note that due to symmetry relations the same percentage error is attained with fewer terms. This is shown by (11b) and (11a). In the first, sign alternation guarantees conversion and reduces the number of terms required for a definite percentage error. In the second, the exclusion of odd values of m gives the same error with a smaller number of terms.

Inspection of theoretical results (Figs. 6, 7, 8) shows that $|Z_a|$ and $|Z_b|$ depend mainly on post width, gap height, and frequency. The effect of gap size is less pronounced. $|Z_c|$, however, depends largely on gap size and height as well as on post width. Its dependence on frequency is less pronounced than that of Z_a and Z_b.

IV. EXPERIMENTAL MEASUREMENTS

As pointed out by Lewin [5] the mount could be tackled either as an antenna system radiating into a waveguide or as a waveguide obstacle.

So far in the theoretical analysis, the posts were considered as antennas radiating in the guide and the driving point impedance at the gap terminals calculated. A direct measure of this impedance presented some practical difficulties; and we opted for testing the structure as a waveguide obstacle, although the impedance level of the obstacle as a shunt element was in many cases low, which rendered accurate impedance measurements difficult.

Thus the structure was matched from one side and impedance measurements carried out.

Measurements were carried on cylindrical posts.

A first set of measurements was carried on posts 1 mm in diameter. With such small diameter, the effect of nonuniform current density distribution in the posts and that of field phase variation across the posts in the z direction are not very pronounced.

Following Eisenhart and Khan [4] an equivalent post width $w = 1.8d$ was postulated and the theoretical results. thus obtained showed a very good agreement between theory and experiment. Better agreement is reached if the nonuniform current distribution across the post is taken into consideration. In fact, if the reactive components of the T coupling circuit for $n = 0$ are multiplied by the factor $[1 - (w/(2a)]$, the experimental results fit almost exactly the theoretical model up to gap widths g of the order of $b/4$.

A second set of measurements was carried on posts 2.5 mm in diameter. In this case, the effect of the phase variation of the field across the posts in the z direction is more evident, since it is proportional to the square of the diameter [7]. It is revealed by the fact that the measured normalized conductance at the post plane is higher than 1 for inductive obstacle reactances and less

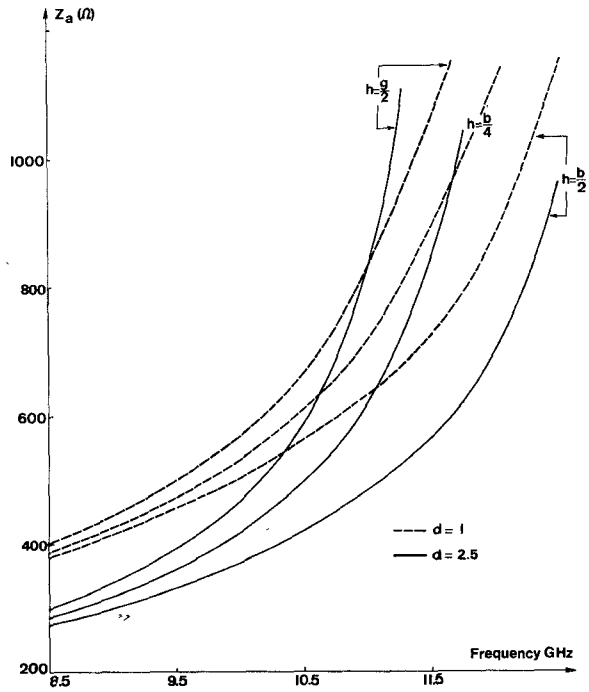

Fig. 6. Theoretical uncorrected frequency dependence of $|Z_a|$ (inductive) for different gap heights (h) (Z_a is referred to the gaps). $a = 22.866$ mm, $b = 10.16$ mm, $s = 5.75$ mm, $g = 1.6$ mm. Dashed curve: $d = 1$ mm. Solid curve: $d = 2.5$ mm.

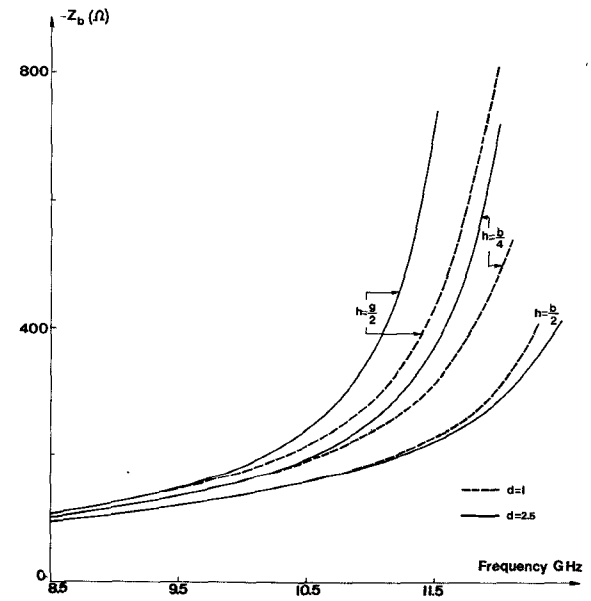

Fig. 7. Theoretical (uncorrected) frequency dependence of $|Z_b|$ (capacitive) for different gap heights (Z_b is referred to the gaps). Dashed curve: $d = 1$ mm. Solid curve: $d = 2.5$ mm.

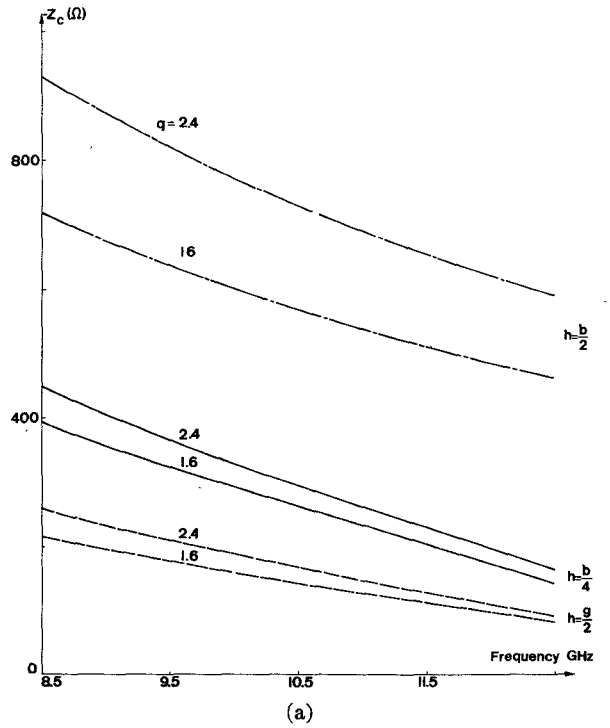

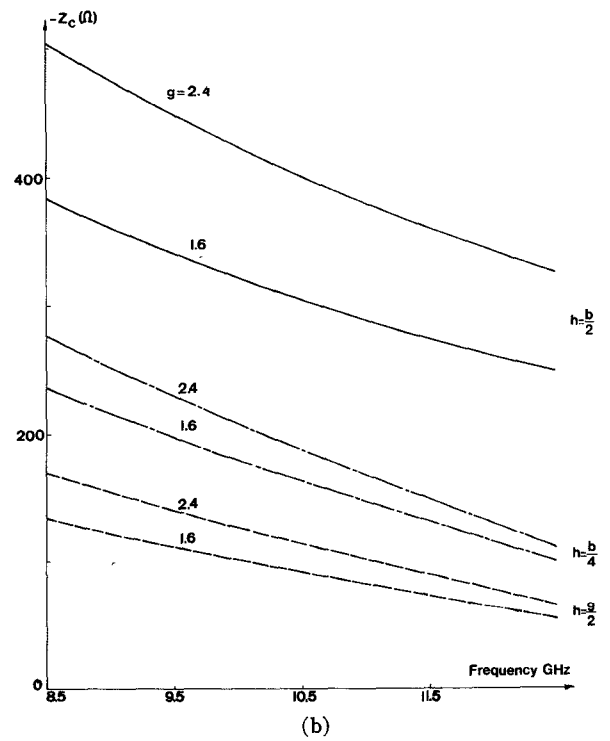

Fig. 8. Theoretical (uncorrected) frequency dependence of Z_c (capacitive) for different gap heights and gap separations. (a) $d = 1$ mm. (b) $d = 2.5$ mm.

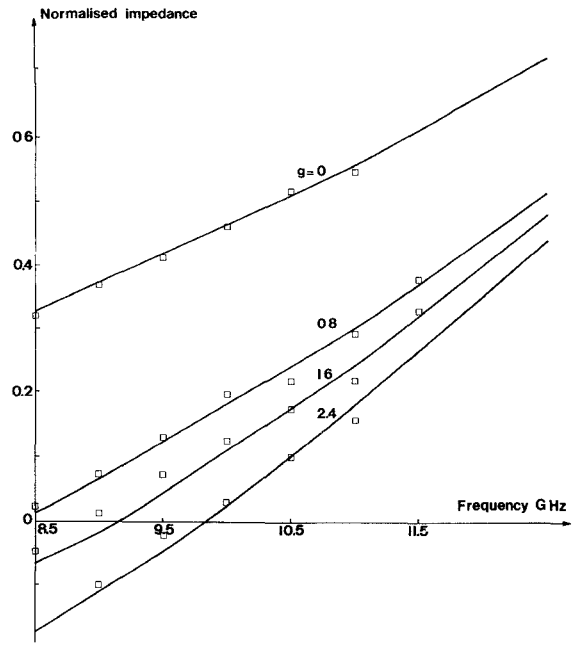

Fig. 9. Theoretical and experimental normalized obstacle equivalent shunt impedance versus frequency for different gap separations with gaps at the bottom of the guide ($h = g/2$), $d = 1$ mm, $s = 5.75$ mm. [The theoretical curves include the correction term $(1 - w/2a)$ and the series reactance X_{sc}.]

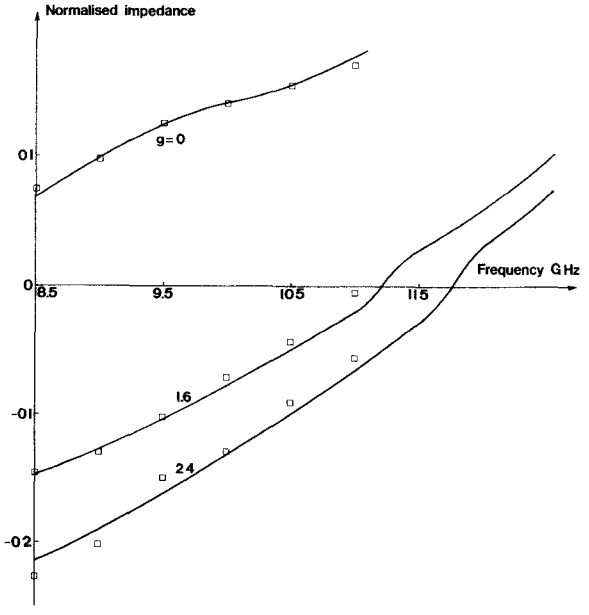

Fig. 10. Theoretical and experimental normalized obstacle equivalent shunt impedance versus frequency for different gap separations with gaps at the bottom of the guide ($h = g/2$), $d = 2.5$ mm, $s = 5.75$ mm. (The theoretical curves include the correction term $(1 - w/2a)$ and the series reactance X_{sc}.)

than 1 for capacitive obstacle reactances. This effect is accounted for by the addition of two capacitive reactances X_{sc} as shown in Fig. 5 where

$$X_{sc} = -2Z_0 \frac{a}{\lambda_g} \left(\frac{\Pi d}{a}\right)^2 \sin^2 \frac{\Pi s}{a}$$

(referred to the center of the guide.) (16)

It is seen from Figs. 9–11 that good agreement is obtained. This is valid up to post diameters of $a/8$ (corresponding to post widths of $a/5$).

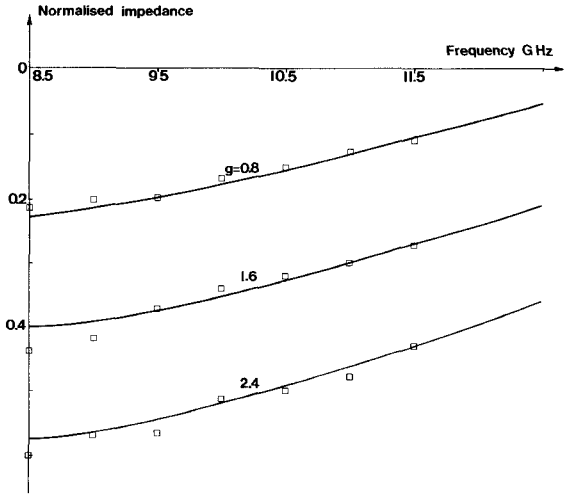

Fig. 11. Theoretical and experimental normalized obstacle equivalent shunt impedance versus frequency for different gap separations with gaps centered in the middle of the guide ($h = b/2$), $d = 2.5$ mm, $s = 5.75$ mm. (The theoretical curves include the correction term $(1 - w/2a)$ and the series reactance X_{sc}.)

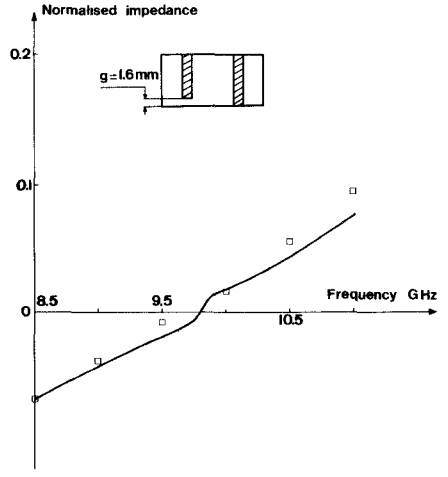

Fig. 12. Theoretical and experimental normalized equivalent shunt impedance of the structure shown versus frequency $d = 2.5$ mm, $s = 5.75$ mm. (The theoretical curves include the correction term $(1 - w/2a)$ and the series reactance X_{sc}.)

Experimental measurements were also carried to test the effect of unequal loading of the gaps. A limiting case, consisting in shorting one gap and leaving the other gap open, was tested and showed good agreement with computations based on the proposed equivalent circuit (Fig. 12).

CONCLUSION

On the basis of the experimental measurements, we may conclude that within the above-mentioned restrictions the proposed lumped equivalent circuit succeeds in providing a fairly good characterization of the considered mounting structure. It provides a reliable tool for the design of parallel varactor-tuned waveguide-mounted Gunn oscillators.

ACKNOWLEDGMENT

The author wishes to thank Prof. J. Herve, Université de Provence (Centre de Saint-Jérôme) and G. Convert, Laboratoire Central Thomson-C.S.F., for many helpful discussions. He also wishes to thank Mr. Mailhan for his technical assistance.

REFERENCES

[1] M. Dean and M. J. Howes, "*J* band transferred-electron oscillators," *IEEE Trans. Microwave Theory Tech.*, vol. MTT-21, pp. 121–127, Mar. 1973.
[2] D. Cawsey, "Wide-range tuning of solid-state microwave oscillators," *IEEE J. Solid-State Circuits* (Corresp.), vol. SC-5, pp. 82–84, Apr. 1970.
[3] *Gunn Diode Circuit Handbook*, Microwave Associates/HB-9000, Feb. 1971, pp. 20–24.
[4] R. L. Eisenhart and P. J. Khan, "Theoretical and experimental analysis of a waveguide mounting structure," *IEEE Trans. Microwave Theory Tech.*, vol. MTT-19, pp. 706–719, Aug. 1971.
[5] L. Lewin, "A contribution to the theory of probes in waveguides," *Proc. Inst. Elec. Eng.*, Monogr. 259R, Oct. 1957.
[6] E. C. Jordan, *Electromagnetic Waves and Radiating Systems*. London: Constable, 1962, pp. 227–228.
[7] N. Marcuvitz, *Waveguide Handbook* (M.I.T. Rad. Lab. Ser., vol. 10). New York: McGraw-Hill, 1951, pp. 258–262.

Modal Analysis of a Planar Dielectric Strip Waveguide for Millimeter-Wave Integrated Circuits

T. T. FONG, MEMBER, IEEE, AND SHUNG-WU LEE, MEMBER, IEEE

Abstract—**A novel planar waveguide which is suitable for guiding electromagnetic (EM) energy in the millimeter-wave and submillimeter-wave regions is studied. By using Wiener–Hopf techniques, we first determine the reflection coefficient at the open ends of the guide. Next, a transverse resonance condition is applied to determine the dispersion relation of the modal field. The propagation constant is found to be complex. Its imaginary part accounts for the edge diffraction loss of the strip through the open ends of the guide. Extensive numerical results are given for the disperson characteristics and modal field distributions for silicon and fuzed quartz substrates. The planar strip waveguide should have the advantages of simplicity in processing, a lower random diffraction loss, and accessibility to monolithic integration techniques.**

I. INTRODUCTION

RECENT rapid advances in millimeter-wave active and passive solid-state devices have made feasible many system applications. In order to develop a functional module for a particular system application and to reduce the size and weight of the module, an integrated circuit approach is of considerable interest. The use of a dielectric waveguide and its associated components has recently been explored in the millimeter wavelength region [1] and some encouraging results have been reported. However, the dielectric waveguide must be fabricated by chemical etching or machining, and suffers from undesirable diffraction loss and phase distortion due to random waveguide variation introduced in the fabrication process. In this paper we study the possibility of using a planar dielectric strip waveguide which does not have the preceding fabrication difficulties. As shown in Fig. 1, the geometry of the strip guide is identical to a microstrip transmission line [2]–[5] which has been widely used at microwave frequencies. Unlike the microstrip, however, the transverse dimensions of the strip guide are relatively large compared to the wavelength and therefore the guide no longer supports the TEM or quasi-TEM mode of propagation characterized by a zero cutoff frequency [2]–[5]. Consequently, despite the geometrical similarity, the modal fields of a strip guide are completely different from those of a microstrip.

It is to be stressed that the substrate thickness for a dielectric strip guide is considerably greater than for a conventional microstrip. Typically, the thickness is ten to fifteen times greater so that dominating TEM or quasi-TEM modes in the microstrip are no longer supported in the strip guide. This results from strong radiation caused by the large substrate thickness. The only modes that can still propagate in the dielectric strip guide are similar to those described by Vainshtein [6], for which the propagation constants in the transverse x direction are small and the waves undergo strong reflections at the open ends. The energy is thus trapped in the waveguide and does not radiate into the free space. Therefore, the strip guide described in this paper is entirely different from the wide microstrip configurations such as the microguide [7] or the edge mode microstrip described by Hines [8]. The greater substrate thickness is advantageous at millimeter and submillimeter wavelengths because of ease in fabrication.

Manuscript received November 5, 1973; revised March 18, 1974.
T. T. Fong is with the Hughes Research Laboratories, Torrance, Calif. 90509.
S.-W. Lee is with the Department of Electrical Engineering, University of Illinois, Urbana, Ill. 61801.